International Journal of Signal Processing, Image Processing and Pattern Recognition
Vol.9, No.3 (2016), pp.61-70
http://dx.doi.org/10.14257/ijsip.2016.9.3.06

An Image Fusion Algorithm Based on Non-subsampled Shearlet Transform and Compressed Sensing

XING Xiaoxue[1], LI Jie[1], FAN Qinyin[2], SHANG Weiwei[1*]

1. College of Information Engineering, Changchun University, Changchun, 130022, China;
2. School of Engineering, Osaka University, Osaka, 5650871, Japan
E-mail: xiaoxue8184@126.com (XING Xiaoxue)
**Corresponding author E-mail: shangww524033@163.com (SHANG Weiwei)*

Abstract

In order to obtain rapid fusion speed, an image fusion algorithm based on Non-subsampled Shearlet Transform (NSST) and Compressed Sensing (CS) is presented. The source images are decomposed with NSST. Based on local area energy, the low-frequency coefficients are fused. The high-frequency coefficients are compressed, fused and reconstructed with CS. Based on global gradient, the measurements of high-frequency coefficients are fused. The inverse NSST is used to get the final fused image. During the fusion course, only the compressed data of the high-frequency coefficients are fused, so the fusion effects can't be affected. At the same time, the running time can be reduced. In this paper, the multi-focus images are used to verify the algorithm effectiveness. The simulation results indicate that the fusion image can be achieved without prior knowledge of the original images. Although the fusion quality is sacrificed when the sampling rate becomes higher, the algorithm can significantly reduce the time cost and hardware requirements. The algorithm provides an idea on how to satisfy the real time requirements in the fusion system.

Keywords: *Image Fusion; NSST; CS; Local Area Energy; Global Gradient;*

1. Introduction

In the field of multi-source image fusion, the time cost of fusion algorithm depends mostly on the amount of data to be processed. The Non-subsampled Shearlet Transform (NSST) is one of the state-of-the-art MGA tools in [1-3], which could realize the truly sparse representation at various directions and different scales of image. NSST could be used to fuse the image to get better fusion effects. When the number of decomposition levels and direction increase, the high-frequency coefficients will become much more and which will greatly increase the consumption of hardware and software.

Compressed sensing (CS), also known as compressive sampling theory, is put forward by Candès and Donoho in [4-6] in 2006. CS can accomplish information compression along with signal sampling simultaneously. The application of CS in the image fusion can reduce the sampling rate, the storage and the computational complexity of the image, and which can effectively reduce the demand for hardware. Therefore, in recent years, many scholars have focused on the study of image fusion algorithm in CS domain in [7-11].

In the paper, a new image fusion algorithm based on the NSST and CS is proposed. On the one hand, NSST can complete multi-scale image decomposition and directional filter which can extract the low and high frequency information of the image; On the other hand, CS can achieve the compression, sensing, fusion and reconstruction of the

* Corresponding Author

ISSN: 2005-4254 IJSIP

directional sub-band coefficients. The algorithm can obtain better fusion effects at a lower sampling rate.

2. Backgrounds

2.1. Non-subsampled Shearlet Transform

When the dimension , the affine systems are expressed in equation (1) in [12-13].

$$A_{AB}(\psi)=\{\psi_{j,l,k}(x)=\left|\det A\right|^{j/2}\psi(B^{l}A^{j}x-k):j,l\in Z,k\in Z^{2}\} \quad (1)$$

Where, both A and B are 2×2 invertible matrices and $\left|detB\right|$=1 . If $A_{AB}(\psi)$ forms a parseval tight framework for $L^{2}(R^{2})$, the elements of the system are called composite wavelets.

Shearlets are defined as follows:

$$SH_{\psi}f(a,s,t)=\left\langle f,\psi_{a,s,t}\right\rangle,a>0,s\in R,t\in R^{2} \quad (2)$$

$\psi_{a,s,t}$ is defined as follows:

$$\psi_{ast}(x)=\left|detM_{as}\right|^{1/2}\psi(M_{as}^{-1}(x-t)) \quad (3)$$

note that

$$M_{as}=B_{s}A_{a}\qquad A_{a}=\begin{pmatrix}a & 0\\ 0 & \sqrt{a}\end{pmatrix}\qquad B_{s}=\begin{pmatrix}1 & s\\ 0 & 1\end{pmatrix} \quad (4)$$

where, A_a is an anisotropic dilation matrix, and B_s is a shear matrix.

The tiling of the frequency plane induced by shearlet and the frequency support comparison of shearlet and wavelet are illustrated in Figure 1. It can be seen from Figure 1 that the frequency support of shearlet transform is a trapezoidal region which is symmetric relatively for the origin along the direction of the slope s in different scales.

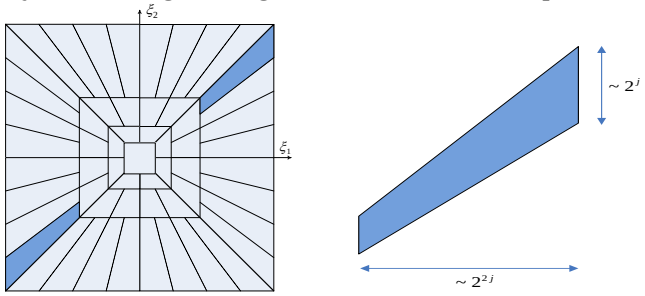

(a) The tiling of the frequency plane (b) supports

Figure 1. The Tiling of the Frequency Plane and Supports of Shearlet

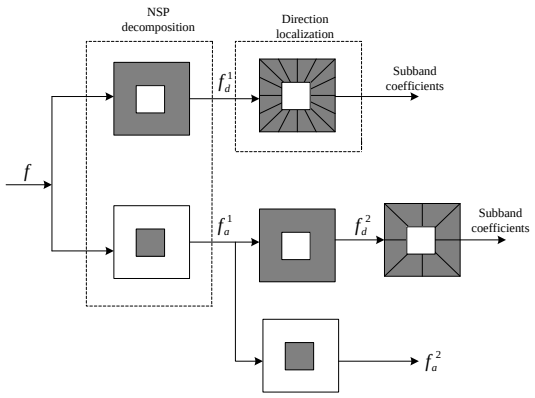

Figure 2. Two Level Decomposition Diagram of NSST

NSST is comprised of multi-scale partition and directional localization in [14-15]. In the multi-scale partition, non-subsampled pyramid decomposition is used to reduce the sensitivity to the image shift. In the directional localization, the frequency plane is decomposed into a low-frequency subband and several trapezoidal high-frequency subbands by the non-subsampled shearing filters. The decomposition structure is shown in Figure 2.

2.2. Compressed Sensing

The CS theory was developed by Candes, Romberg, Tao and Donoho. CS theory shows that if a signal can be represented sparsely, with far less than the number of the observations required by the Nyquist sampling theorem, the original signal can be accurately reconstructed. The process concludes 3 parts: signal sparse representations, signal measurements and signal reconstruction.

The system diagram of CS theory is shown in Fig.3.

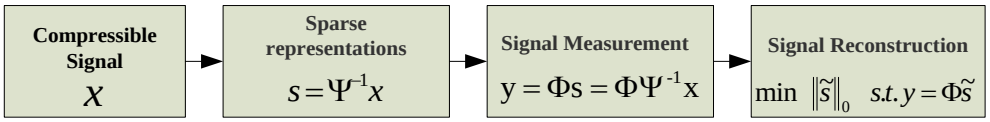

Figure 3. The System Diagram of CS Theory

The four main implementation steps are as follows:

Step 1: Represent the original signal x sparsely in a certain domain Ψ.

$$x = \Psi s \qquad or \qquad x = \sum_{i=1}^{N} S_i \Psi_i \tag{5}$$

where, $\Psi = [\Psi_1, \Psi_2, \cdots, \Psi_N]$, S is the sparse representation of x.

Step 2: Design a measurement matrix $\Phi(M << N)$ unrelated to Ψ to accomplish the linear transformation of s. The measurement result is y.

$$y = \Phi s = \Phi \Psi^{-1} x \tag{6}$$

Step 3: Calculate the sparse signal $\tilde{s}$ according to y, Φ, Ψ.

$$\min \|\tilde{s}\|_0 \quad s.t. \quad y = \Phi \tilde{s} \tag{7}$$

Step 4: Reconstruct the original signal x .

$$\tilde{x} = \Psi\tilde{s} \quad (8)$$

3. Proposed Fusion Algorithm

It can be seen that the low-frequency coefficients don't have sparsity, so in proposed algorithm only the high-frequency coefficients will to be deal with by CS after the decomposition of the original images with NSST. The coefficients of low frequency and high frequency are processed separately which can get better fusion effects.

3.1. Fusion Framework

The block diagram of the image fusion in CS based on NSST is shown in Figure 4. LFC represents the low-frequency components. HFC represents the high-frequency components.The original images are A and B. The fused image is F. The specific steps of image fusion based on NSST and CS are as follows:

Step 1: Image A and B should be registrated.

Step 2: A and B are decomposed with NSST to obtain $\{AL, AH^{j,k}\}$ and $\{BL, BH^{j,k}\}$. AL and BL represent separately the low-frequency coefficients of A and B. $AH^{j,k}$ and $BH^{j,k}$ represent the k^{th} high-frequency sub-band coefficients in the j^{th} decomposition layer of A and B.

Step 3: AL and BL are weighted by local area energy.

Step 4: The sampling rate is M / N . Gaussian random matrix is used to observe $AH^{j,k}$ and $BH^{j,k}$, the measurements are $y_{AH}^{j,k}$ and $y_{BH}^{j,k}$.

Step 5: $y_{AH}^{j,k}$ and $y_{BH}^{j,k}$ are weighted by global gradient to get the observed value $y_{FH}^{j,k}$.

Step 6: The orthogonal matching pursuit (OMP) algorithm is used to reconstruct $FH^{j,k}$.

Step 7: The inverse NSST is used to obtain the final fused image.

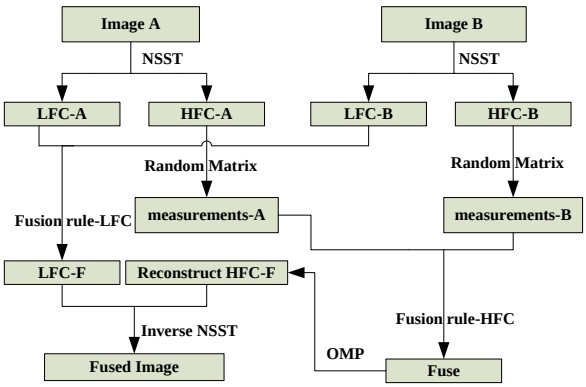

Figure 4. The Diagram of Fusion Dcheme

3.2. Fusion Rules of the Low-Frequency Coefficients

Concentrating on the main energy of the image, the low-frequency components reflect the approximate and average characteristics of the image, which can't be processed by CS due to the absence of sparse feature. Therefore, in this paper, the the low-frequency coefficients of the image are fused based on weighted local area energy.

$AL(r,c)$ and $BL(r,c)$ are the low-frequency coefficients of A and B. $E_{AL}(r,c)$ and $E_{BL}(r,c)$ are the local regional energy. The calculation formulas are shown in formula (9) to (10).

$$E_{PL}(r,c)=\sum_{(m,n)\in\Omega(r,c)} w(m,n)[f_{PL}(m,n)]^2, \qquad P=A,B$$

(9)

$$w=\frac{1}{15}\begin{Bmatrix}1 & 2 & 1\\ 2 & 3 & 2\\ 1 & 2 & 1\end{Bmatrix}$$

(10)

where, $\Omega(r,c)$ is a 3×3 neighborhood window centered on (r,c). $f_{PL}(m,n)$ is the gray value at the pixel (m,n). $w(m,n)$ is window function.

The low frequency coefficients $FL(r,c)$ of fused image can be calculated based on formula (11).

$$FL(r,c)=\begin{cases} AL(r,c), & E_{AL}(r,c)>E_{BL}(r,c)\\ \omega_A(r,c)AL(r,c)+\omega_B(r,c)BL(r,c), & else\\ BL(r,c), & E_{AL}(r,c)\le E_{BL}(r,c)\end{cases}$$

(11)

where, $\omega_A(r,c)$ and $\omega_B(r,c)$ satisfy formula (12).

$$\begin{cases}\omega_A(r,c)=\dfrac{E_{AL}(r,c)}{E_{AL}(r,c)+E_{BL}(r,c)}\\ \omega_B(r,c)=1-\omega_A(r,c)\end{cases}$$

(12)

3.3. The Fusion of the High-Frequency Coefficients

Most of the high-frequency coefficients obtained from NSST decomposition fluctuate around zero, and only a small part has larger amplitude. Therefore, based on the CS theory it can be considered that high-frequency coefficients have large sparsity, and which can be compressed to speed up the running speed and reduce time loss.

Gaussian random matrix is used to observe the high-frequency coefficients $AH^{j,k}$ and $BH^{j,k}$, and the measurements are $y_{AH}^{j,k}$ and $y_{BH}^{j,k}$, which is given by:

$$y_{PH}^{j,k}=\Phi\times PH^{j,k}, \qquad P=A,B$$

(13)

The gradient image of $y_{AH}^{j,k}(p)$ and $y_{BH}^{j,k}(p)$ are $G_{AH}^{j,k}(p)$ and $G_{BH}^{j,k}(p)$, which is given by:

$$G_{PH}^{j,k}(p)=\nabla_x^2 y_{PH}^{j,k}(p)+\nabla_y^2 y_{PH}^{j,k}(p), \qquad P=A,B$$

(14)

Based on the global gradient, the measurements image $y_{FH}^{j,k}(p)$ after fusion is given by:

$$y_{FH}^{j,k}(p)=\begin{cases} y_{AH}^{j,k}(p) & G_{AH}^{j,k}(p)>G_{BH}^{j,k}(p)\\ y_{BH}^{j,k}(p) & G_{AH}^{j,k}(p)<G_{BH}^{j,k}(p)\\ \omega\times y_{AH}^{j,k}(p)+(1-\omega)y_{BH}^{j,k}(p) & \text{else}\end{cases}$$

(15)

$$\omega = \frac{\left|\sum_k \frac{1}{n_R}\sum_{p\in R} G_{AH}^{j,k}(p)\right|}{\left|\sum_k \frac{1}{n_R}\sum_{p\in R} G_{AH}^{j,k}(p)\right| + \left|\sum_k \frac{1}{n_R}\sum_{p\in R} G_{BH}^{j,k}(p)\right|} \qquad k = \{k_1, k_2, \cdots, k_q\}, \qquad j = 1,2,3 \tag{16}$$

where, R is a rectangular area with $n \times m$, $n_R = n \times m$, and it usually is 3×3 . Set $j \hat{I} \{1,2,3\}$, $j = 1, k = \{1,2,3,4\}$; $j = 2, k = \{1,2,3,4\}$; $j = 3, k = \{1,2,L\ ,8\}$.

4. Experimental Results and Discussion

In this section, the multi-focus images shown in Figure 5 are provided to demonstrate the effectiveness of the proposed method. The other four algorithms, including NSST-based algorithm, CS-based algorithm, DWT-CS-based algorithm in [16], and NSCT-CS-based algorithm in [17], are used to compare with our proposed approach.

The images are all decomposed into 3 levels by DWT (with the basis of Sym8), NSCT and NSST. The pyramid filter for NSST and NSCT is set as 'maxflat ' and the directional filter for NSCT is set as 'dmaxflat'. The high-frequency coefficients images are all sparsified with wavelet sparse matrix, observed with Gaussian random matrix and reconstructed using OMP algorithm. For all the algorithms, the fusion rule adopts the fusion method proposed in this paper. The fusion results are shown in Figure 6 and Figure 7.

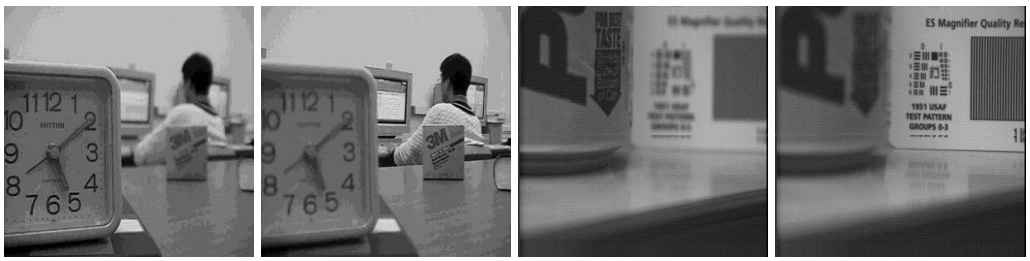

(a) Lab1 (b) Lab2 (c) Pepsi1 (d) Pepsi2

Figure 5. Multi-Focus Source Images

The subjective visual perception gives us direct comparisons, and some objective image quality assessments are also used to evaluate the performance of the proposed approach. The following image quality metrics are used in this paper: Entropy (E), Average gradient (AG), Standard deviation (SD), edge information retention capacity ($Q^{AB/F}$), spatial frequency (SF) and the algorithm time consuming (T). The results are shown in Table 1 and Table 2.

From Figure 6 and Figure 7 we can see that image fusing using NSST-CS can obtain a fusion image, on which more detail information, disperse the gray level and higher sharpness can be seen clearly. From Table 1 and Table 2, we can see that NSST-CS can get a least consumption time and better results. Therefore fusion image based on NSST-CS has many advantages over other methods on multi-focus image fusion.

(a) NSST (b) CS (c) DWT-CS

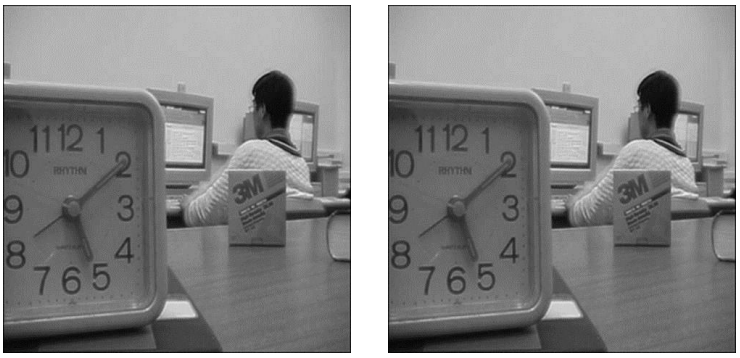

(d) NSCT-CS (e) NSST-CS

Figure 6. Fusion Results on "Lab" Image

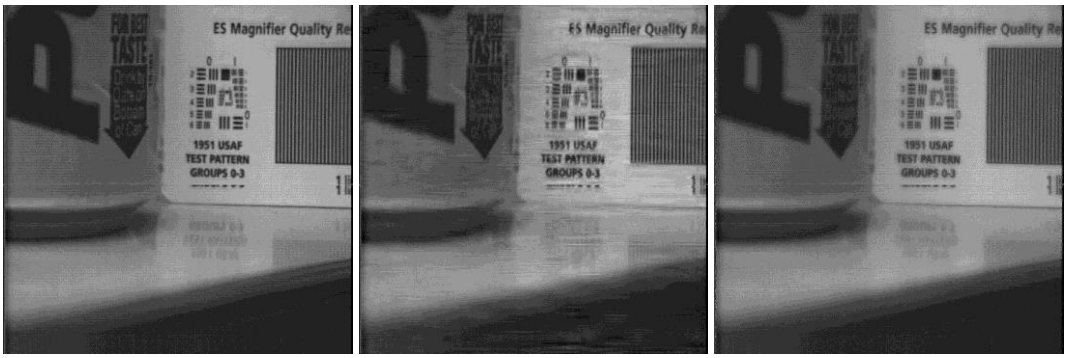

(a) NSST (b) CS (c) DWT-CS

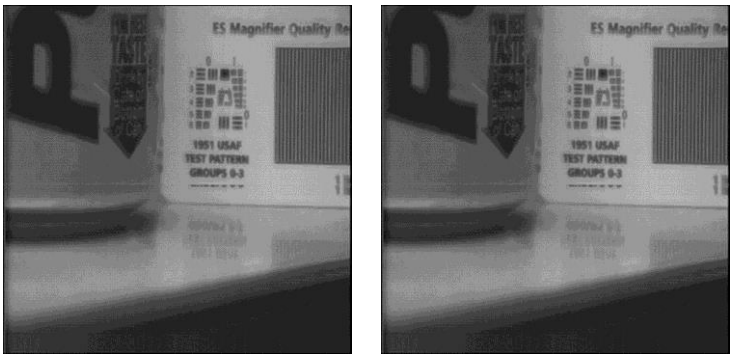

(d) NSCT-CS (e) NSST-CS

Figure 7. Fusion Results on "Pepsi" Image

Table 1. Comparison of Multi-Focus "Lab" Image

	E	AG	$Q^{AB/F}$	SF	SD	T(s)
NSST	7.3768	7.0008	0.6784	14.2745	45.8116	48.0346
CS	5.0736	3.5800	0.3643	11.2772	48.5338	11.7172
DWT-CS	7.0218	4.1166	0.4479	11.2860	47.7095	30.5218
NSCT-CS	7.0520	4.9339	0.5155	13.2112	47.2986	34.2837
NSST-CS	**7.1658**	**5.1649**	**0.5414**	**13.8109**	**46.1115**	**24.7591**

Table 2. Comparison of Multi-Focus "Pepsi" Image

	E	AG	$Q^{AB/F}$	SF	SD	T
NSST	7.2957	5.9043	0.7403	14.8624	43.1001	72.9606
CS	5.0940	3.0026	0.3679	8.1198	46.1302	16.3769
DWT-CS	7.0974	4.0804	0.4198	12.6476	45.2816	40.2357
NSCT-CS	7.0962	4.7217	0.4522	13.5746	45.2391	49.7327
NSST-CS	**7.1512**	**4.9457**	**0.4849**	**13.6946**	**44.1670**	**35.1546**

5. Conclusion

Although NSST can extract more effective detail information of the multi-focus images, it also brings the processing problem of the large amount of high-frequency decomposition coefficients. The CS technology applied in the high-frequency decomposition image fusion can reduce the calculation amounts and quicken the fusion speed. The experimental results show that the fusion image can be achieved without prior knowledge of the original images. The method based on NSCT and CS has better fusion results, lower computational complexity and fewer requirements for the hardware system. The method provides an idea on how to satisfy the real time requirements in the fusion system, and which has great application value.

Acknowledgements

The authors would like to thank for the developers of the shearlet toolbox, wavelet toolbox and the NSCT toolbox. This work is supported by Jilin Province Education Department (No. 20140529) and the "Chunhui" Project of the National Ministry of Education (No. Z2014138).

References

[1] G. Easley and D. Labate, W. Q. Lim, "Sparse directional image representations using the discrete shearlet transform", Applied Compution Harmonic Analysis, vol. 25, no. 1, **(2008)**, (1)pp. 25-46.
[2] K. Guo and D. Labate, "Optimally Sparse Multidimensional Representation using Shearlets", SIAM JMathl Anal, vol. 39, **(2007)**, pp. 298-318.
[3] T.T, Bai, C-X Deng and Y. Geng, "Image Edge Detection Based on Wavelet Transform and Canny Operator", Journal of Harbin University of Science and Technology, vol. 15, no.1, **(2010)**, pp. 44-48.
[4] Candes E. J., "Compressive Sampling", In Proc. Int. Congress of Math., Madrid, Spain, **(2006)**, pp. 1433-1452.
[5] Donoho D. L., "Compressed Sensing", IEEE Transactions on Information Theory, vol. 52, no.4, **(2006)**, pp. 1289-1306.
[6] J.Gai, Z. Tong, C. Kun and Z. Liu, "A Compressible Sampling Method of Spectrom-sparse Signal", Journal of Harbin University of Science and Technology, vol. 18, no.6, **(2013)**, pp. 64-68.
[7] Wan T., Canagarajah N. and Achim A., "Compressive Image Fusion", Proc of IEEE International Conference on Image Processing, (2008), pp. 1308-1311.

[8] Luo X., Zhang J. and Yang J., "Image Fusion in Compressed Sensing", IEEE Int Conf on Image Processing, **(2009)**, pp. 2205-2208.
[9] Han J. J., Otmar L. and Klaus H., "Multi image fusion based on compressive sensing", International Conference on Audio Language and Image Processing, **(2010)**, pp. 1463-1469.
[10] Liu G. and Shen Y., "Ultrasonic image fusion using compressed sensing", Electronics Letters, Vol.48, no. 19, **(2012)**, pp. 1182-1184.
[11] Li S. T., Yin H. T. and Fang L. Y., "Remote Sensing Image Fusion via Sparse Representations Over Learned Dictionaries", IEEE Transactions on Geosciences and Remote Sensing, vol. 51, no. 9, **(2013)**, pp. 4779-4789.
[12] Guo K. and Labate D., "Optimally Sparse Multidimensional Representation using Shearlets", SIAM JMathl Anal, Vol. 39, **(2007)**, pp. 298-318.
[13] Easley G., Labate D. and Lim W., "Sparse Directional Image Representation using the Discrete Sheralet Transform", Appl Comput Harmon Anal, vol. 25, no. 1, **(2008)**, pp. 25-46.
[14] Wang L., Li B. and Tian L. F., "Medical Image Fusion Based on Shift-Invariant Shearlet Transformation", Journal of South China University of Technology (Natural Science Edition), vol. 39, no.12, **(2011)**, pp.13-19.
[15] Gao Y. H., Chen G. Q. and Liu Y. Y., "Adaptive image fusion based on image quality assessment parameter in NSST domain", Journal of Jilin University (Engineering and Technology Edition), vol. 43, no.1, **(2014)**, pp. 225-234.
[16] Y. T. Yang, "The Image Fusion Based on Non-subsampled Contourlet Transform", Graduate of Chinese academy of sciences, Ph.D. Thesis, **(2012)**.
[17] Y. Shen, "A Improved Image Fusion Algorithm Based on Wavelet Transform", Automation and Instrumentation, no.5, **(2013)**, pp. 202-204.

